Robotica: (2019) volume 37, pp. 2132–2146. © Cambridge University Press 2019
doi:10.1017/S0263574719000948

Human Evaluation of Wheelchair Robot for Active Postural Support (WRAPS)

Chawin Ophaswongse†, Rosemarie C. Murray†, Victor Santamaria†, Qining Wang‡ and Sunil K. Agrawal†*

†*Robotics and Rehabilitation Laboratory (ROAR Lab), Department of Mechanical Engineering, Columbia University, New York, NY 10027, USA.*
E-mails: co2393@columbia.edu, rcm2146@columbia.edu, vs2578@columbia.edu
‡*The Robotics Research Group, College of Engineering, Peking University, Beijing 100871, China.*
E-mail: qiningwang@pku.edu.cn

(Accepted May 25, 2019. First published online: January 26, 2019)

SUMMARY
People with severe neuromuscular trunk impairment cannot maintain or control upright posture of the upper body in sitting while reaching. Passive orthoses are clinically available to provide support and promote the use of upper extremities in this population. However, these orthoses only position the torso passively without any degree of trunk movement.

We introduce for the first time a novel active-assistive torso brace called Wheelchair Robot for Active Postural Support (WRAPS). It consists of two rings over the hips and chest connected by a 2RPS-2UPS parallel robotic device. WRAPS can modulate the displacement of the upper ring and/or the forces applied on the torso through the ring in four degrees-of-freedom (DOF), including rotations and translation in the sagittal and frontal planes.

In the present study, we evaluate the design of WRAPS and its functions. Moreover, we discuss the potential effectiveness of WRAPS as a therapeutic robotic tool in people with severe trunk control deficits. The performance of WRAPS was evaluated in seated healthy subjects. Kinematics and surface electromyography (sEMG) were collected when the participants performed selective trunk movements. First, the torso range of motion (tROM) was calculated with WRAPS in transparent mode—zero-force control mode—which was compared with free-guided tROM (no WRAPS) with motion capture system. Second, a position control mode was configured to mobilize the torso along the trajectories obtained with the transparent mode.

Our results show that the design of WRAPS suited well the subject's anthropometrics while supporting the weight of the torso. Importantly, WRAPS can be programmed to replicate the subject's tROM, without the full activation of torso muscles. This can be critical in individuals with no trunk control. Altogether, these preliminary results indicate the potential applicability of WRAPS to promote active-assistive trunk mobility in people who cannot sit independently because of trunk dysfunction.

KEYWORDS: Wearable robotics; Exoskeletons; Parallel manipulators; Trunk impairment; Human biomechanics.

1. Introduction

For most people, sitting up independently and performing everyday tasks, such as picking up objects from a shelf, using a computer, or eating while seated, do not require a second thought. However, for people without trunk control, these day-to-day seated tasks are unachievable. Particularly, this is true

* Corresponding author. E-mail: sa3077@columbia.edu

https://doi.org/10.1017/S0263574719000948 Published online by Cambridge University Press

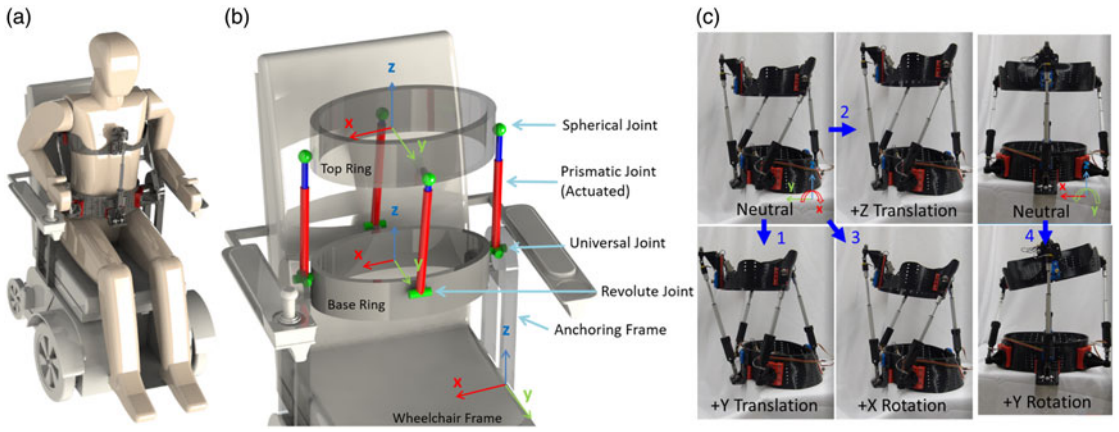


Fig. 1. (a) CAD drawing of the overall system with a user in the WRAPS on a wheelchair. (b) WRAPS has four controlled DOFs based on the 2RPS-2UPS parallel architecture. (c) Motions in each of the four DOFs.

for people with spinal cord injury (SCI) in the cervical and high-thoracic regions, among those with other pathologies such as spina bifida, neuromuscular diseases, or cerebral palsy.

The number of people in the USA who are living with SCI is estimated to be 300,000 in 2018.[1] People with severe SCI show flaccid trunk control and muscle spasms that limit their ability to sit independently and functionally perform upper extremity tasks within arm's distance or beyond maximum arm's extension. Additionally, people with profound poor trunk control are always at risk of falling from the wheelchair while reaching and as a result may choose to avoid these activities due to fear of potential injuries.[2,3]

Most of the present rehab equipment for people with severe SCI, including straps, thoracolumbosacral orthoses, and tilt wheelchairs, are passive and constrain the trunk to only reach within arm's distance. Consequently, the workspace surrounding these individuals and their motor flexibility in reaching is highly restricted. As a result, functional independence of wheelchair users with severe SCI is substantially compromised. Also, from a rehabilitation standpoint, this situation is not ideal because the person has limited use of the arms within the peripersonal space and limited opportunity to move the trunk further from the base of support. Furthermore, people with SCI at level T6 or higher struggle to shift their body weight within their base of support to prevent vascular stasis and often develop comorbidities such as pressure ulcers, deep vein thrombosis, and autonomic dysreflexia.[4] The lack of functional independence during sitting and the need to prevent vascular-related events make people with SCI on wheelchairs rely heavily on caregiver assistance. New passive orthotic systems provide greater range of motion of the upper body, see, for example, Refs. [5, 6]. However, these devices are not designed to actively assist the control of rotation and translation of the torso in seated functional tasks.

Keeping in mind this functional and vascular need in the population with SCI and severe trunk dysfunction, we have developed and tested in able-bodied people a novel active brace, the Wheelchair Robot for Active Postural Support (WRAPS).[7] The overall 3D CAD model of the system is shown in Fig. 1(a). The robot consists of four kinematic chains in parallel between the pelvic and thoracic rings, as shown in Fig. 1(b). The robot has four active degrees-of-freedom (DOF) to accommodate the flexion-extension motion in the sagittal plane ($y-z$ translation and x rotation), as well as lateral rotation (around y-axis) (Fig. 1(c)). The device is currently designed so that it does not allow lateral translation of the trunk or axial rotation. These features were added to curtail vertebral lateral instability that may promote the development of neuromuscular scoliosis in the frontal plane. From Fig. 1(b), the kinematic chains in the front and back of the user have a Revolute, Prismatic, and Spherical (RPS) joint structure. The chains on the sides have a Universal, Prismatic, and Spherical (UPS) joint structure. Together, these make an overall 2RPS-2UPS parallel structure. Driven by four linear actuators (denoted by P), the device can modulate the displacement of the upper ring and/or the forces applied on the upper torso. Therefore, the device will allow users to sit upright and actively lean forward in the sagittal plane to reach out for objects. The workspace has been developed based on International Organization for Standardization (ISO) anthropometric data. We believe that people with SCI at high-thoracic or low-cervical injury could benefit by using WRAPS.

https://doi.org/10.1017/S0263574719000948 Published online by Cambridge University Press

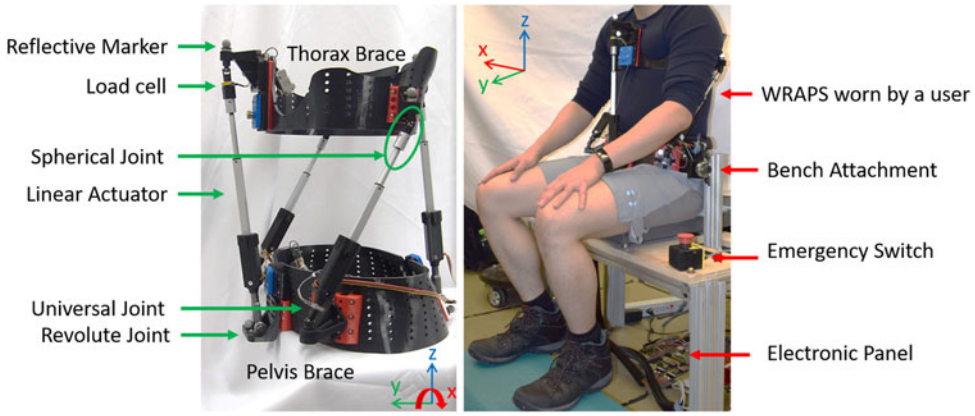


Fig. 2. Hardware configuration of the WRAPS system.

In this study, WRAPS design and performance were evaluated in seated able-bodied subjects. We address three research aims:

1. to characterize the torso range of motion (tROM) of users when wearing WRAPS in comparison to free-guided tROM without wearing it,
2. to determine the active-assistive capability of WRAPS to move the subjects on their own tROM trajectories while reducing activity of their primary torso muscles, and
3. to characterize the relationship between spatiotemporal features of muscle activation during the transparent mode and assistive sagittal forces and moment provided by WRAPS during the assistive mode.

2. Materials and Methods

2.1. Hardware configuration

The overall hardware configuration of that WRAPS is shown in Fig. 2. Two rings were designed from a body scan of a healthy male adult and were 3D-printed with ABS plastic (Fortus 360mc, Stratasys, Eden Prairie, MN, USA). The rings have adjustable widths and have an inner lining of a soft foam pad (Rolyan Polycushion Padding Sheet, Performance Health, Warrenville, IL, USA) to distribute radial pressure and improve wearer comfort. The device is actuated by micro-linear actuators (L16-140-150-12-P in the RPS limbs and L16-100-150-12-P in the UPS limbs, Actuonix Motion Devices, Victoria, BC, Canada). The motors are driven at 12 V using a 1000 Hz PWM signal through a small driver (TB6612FNG, Toshiba, Minato, Tokyo, Japan). These motors contain on-board potentiometers, placed in series with load cells (LCM 200 Miniature Tension and Compression Load Cell with IAA100 Analog Amplifier with Voltage Output, FUTEK, Irvine, CA, USA). The signals from these sensors are multiplexed and sent to a portable reconfigurable I/O (RIO) device (myRIO-1900, National Instruments, Austin, TX, USA) as a control board. Second-order low-pass Butterworth filters were used to smooth the raw signals from the load cells (0.45 Hz cutoff) and the potentiometers (2 Hz cutoff). The command is sent from a user interface of a LabVIEW^{TM} software (version 2017, National Instruments, Austin, TX, USA) in a host computer connected to the control board either through the Wi-Fi or a USB cable. Note that the linear actuators were selected such that the system is not back-drivable, that is, we selected a motor back-drive force at 102 N, which is greater than the expected peak interaction forces with the wearer along all the linear actuators. Hence, the interaction forces between the robot and the wearer can be directly measured by the in-line load cells. The pelvic ring is attached to a custom-made bench by two bearings so that this rotation will accommodate the pelvic tilt during sitting. Alternatively, the bearing shaft can be rigidly fixed relative to the bench in any angle, as needed during experimentation.

https://doi.org/10.1017/S0263574719000948 Published online by Cambridge University Press

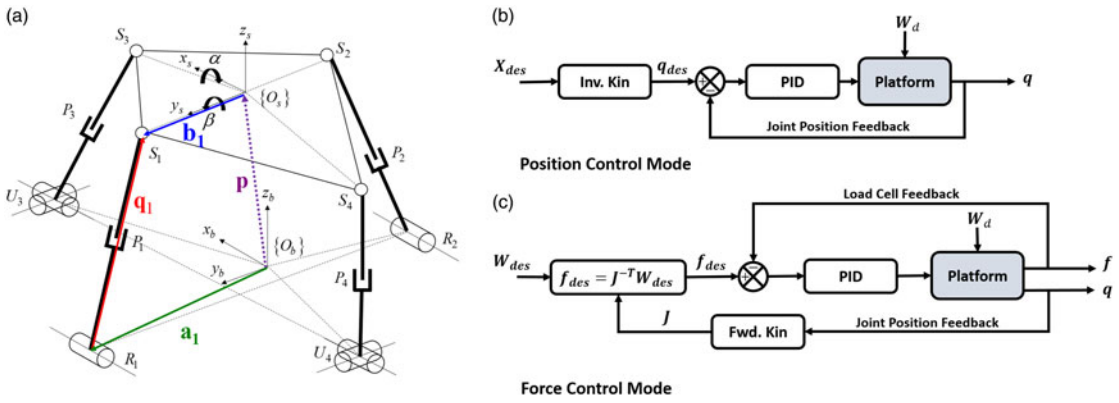


Fig. 3. Kinematics diagram of (a) 2RPS-2UPS parallel mechanism. (b) Position control mode. (c) Force control mode.

2.2. *Mathematical models*

The kinematic diagram of the spatial 2RPS-2UPS parallel mechanism is shown in Fig. 3(a). The plane formed by the centers of the two revolute joints (R_1 and R_2) and the origin of the fixed base coordinate frame $\{O_b\}$ is aligned with the sagittal plane of the body ($y_b - z_b$ plane). The origin of the end-effector coordinate frame $\{O_s\}$ lies on the line connecting the spherical joint centers (S_1 and S_2) of the two RPS limbs, and thus the origin of the end-effector frame is always in the sagittal plane. In addition, the y_s axis is also parallel to the line S_1S_2. $\boldsymbol{a}_i$ are the vectors of joint positions (R_1, R_2, U_3, U_4) with respect to the base frame $\{O_b\}$, while $\boldsymbol{b}_i$ are the vectors of the spherical joint positions (S_1, S_2, S_3, S_4) with respect to the local frame $\{O_s\}$. The position and orientation of the end-effector frame $\{O_s\}$ with respect to the base frame $\{O_b\}$ are fully determined by four variables (y, z, α_x, β_y). y and z are the coordinates of the origin of the end effector frame $\{O_s\}$ relative to the origin of the base frame $\{O_b\}$. α_x and β_y are the first two Euler angles in the body-three 1-2-3 set of orientation angles of the end-effector frame $\{O_s\}$ (rotation around the current x_s axis and then y_s axis, respectively).

Given these four independent variables representing a desired configuration $\boldsymbol{X}_{des} = [y, z, \alpha_x, \beta_y]^T$, the inverse kinematics solution can be solved analytically by using four closed-loop equations to obtain the set of limb lengths, namely

$$\begin{aligned} &\boldsymbol{q}_i = \boldsymbol{p} + \boldsymbol{R}\boldsymbol{b}_i - \boldsymbol{a}_i \quad (i = 1, 2, 3, 4) \\ &q_i = \|\boldsymbol{q}_i\| = \left[(\boldsymbol{p} + \boldsymbol{R}\boldsymbol{b}_i - \boldsymbol{a}_i)^T(\boldsymbol{p} + \boldsymbol{R}\boldsymbol{b}_i - \boldsymbol{a}_i)\right]^{1/2} \end{aligned} \tag{1}$$

where $\boldsymbol{p} = [0, y, z]^T$, and $\boldsymbol{R} = \begin{bmatrix} c\beta_y & 0 & s\beta_y \\ s\alpha_x s\beta_y & c\alpha_x & -s\alpha_x c\beta_y \\ -c\alpha_x s\beta_y & s\alpha_x & c\alpha_x c\beta_y \end{bmatrix}$ ($s\theta := \sin\theta$; $c\theta := \cos\theta$)

The forward kinematics solution is calculated by using the Newton–Raphson algorithm (Ref. [8]). The iterative solution is used as the initial guess at the next time step to minimize the computation time and obtain continuous solutions.

The forces and moments in six DOF $\boldsymbol{W} = [F_x, F_y, F_z, M_x, M_y, M_z]^T$ at the origin of the end-effector with respect to the base frame can be calculated from the vector of joint forces $\boldsymbol{f}$ as follows:

$$\boldsymbol{W} = \boldsymbol{J}_s{}^T \boldsymbol{f} \tag{2}$$

where J_s is the screw-based velocity Jacobian, derived by taking the orthogonal product of each selected reciprocal screw and the instantaneous twist of its respective limb. The selected reciprocal screw is reciprocal to all passive joint screws in the instantaneous twist equation, except for its respective actuated joint screw.[9] For a 2RPS-2UPS mechanism, the screw-based velocity Jacobian is in the following form (Ref. [10]):

https://doi.org/10.1017/S0263574719000948 Published online by Cambridge University Press

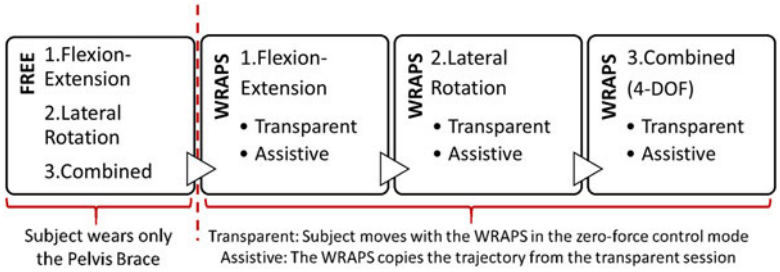


Fig. 4. Experiment Protocol

$$\boldsymbol{J}_s = \begin{bmatrix} \hat{\boldsymbol{q}}_1^{\,T} & \left(\boldsymbol{R}\boldsymbol{b}_1 \times \hat{\boldsymbol{q}}_1\right)^T \\ \vdots & \vdots \\ \hat{\boldsymbol{q}}_4^{\,T} & \left(\boldsymbol{R}\boldsymbol{b}_4 \times \hat{\boldsymbol{q}}_4\right)^T \\ \hat{\boldsymbol{x}}^T & \left(\boldsymbol{R}\boldsymbol{b}_1 \times \hat{\boldsymbol{x}}\right)^T \\ \hat{\boldsymbol{x}}^T & \left(\boldsymbol{R}\boldsymbol{b}_2 \times \hat{\boldsymbol{x}}\right)^T \end{bmatrix}_{6\times 6} \tag{3}$$

where $\hat{\boldsymbol{q}}_i$ are unit vectors along the lines of the actuated prismatic joints (P_1, P_2, P_3, P_4), and $\hat{\boldsymbol{x}} = [1, 0, 0]^T$ is the unit vector along both passive revolute joints at the base platform (R_1 and R_2).

From the Jacobian in (3), one can easily observe that the wrench components in the sagittal plane (F_y, F_z, M_x) are fully determined by the forces measured from the four load cells along the limbs (f_1, f_2, f_3, f_4), while the other components of forces and moments need to be calculated from the unmeasured constraint forces along the revolute joint axes. Hence, the force measurement will be collected only in the sagittal plane components, and the dimension of the Jacobian transpose $\boldsymbol{J}^T$ being used can be reduced to 3×4.

2.3. Controllers

There are two main types of controllers that were implemented. First, in the position control mode shown in Fig. 3(b), the desired joint positions ($\boldsymbol{q}_{des}$) are calculated by inverse kinematics in (1), and then fed to a closed-loop proportional–integral–derivative (PID) controller using the actual joint position of each linear actuator ($\boldsymbol{q}$). Second, in the force control mode in Fig. 3(c), we calculate the required force along each limb ($\boldsymbol{f}_{des}$) from the desired wrench applied by the top ring ($\boldsymbol{W}_{des} = [F_y, F_z, M_x]^T$) and Jacobian ($\boldsymbol{J}$) based on the current robot configuration, and then we use a closed-loop PID controller with feedback from the load cells on the joint level ($\boldsymbol{f}$). Note that $\boldsymbol{W}_d$ is the wrench disturbance on the end-effector from the environment, including the user.

2.4. Experimental protocol

The experiment was approved by the Institutional Review Board (IRB) of Columbia University (Protocol No. AAAP7105). Five healthy adult male subjects participated in the study with an average age of 26.60 years old (SD = 3.05 years, range = 22–29 years old), 71.55 kg average weight (SD = 9.41 kg, range = 60–83 kg), 175.44 cm average height (SD = 7.67 cm, range = 167–184 cm), and 53 cm average torso height (SD = 3.08 cm, range = 51–58 cm) measured from the greater trochanter level to the suprasternal notch. The recruited subjects were within the adjustable range of the WRAPS brace sizes.

The experiment protocol is illustrated by the diagram in Fig. 4. In the "free" session, the subjects were constrained to the bench by the pelvic brace that is rigidly attached to it, while the upper trunk was unrestricted as shown in Fig. 5(a). The subjects were instructed to move the torso relative to the pelvis in flexion-extension (main sagittal plane movement), lateral rotation (main frontal plane), and combined both planes of motion. The subjects were asked to perform the tROM in the given direction, starting from upright seating posture. A total of six continuous cycles were performed in each plane of motion. Additionally, a metronome was used to ensure a constant speed during movement.

https://doi.org/10.1017/S0263574719000948 Published online by Cambridge University Press

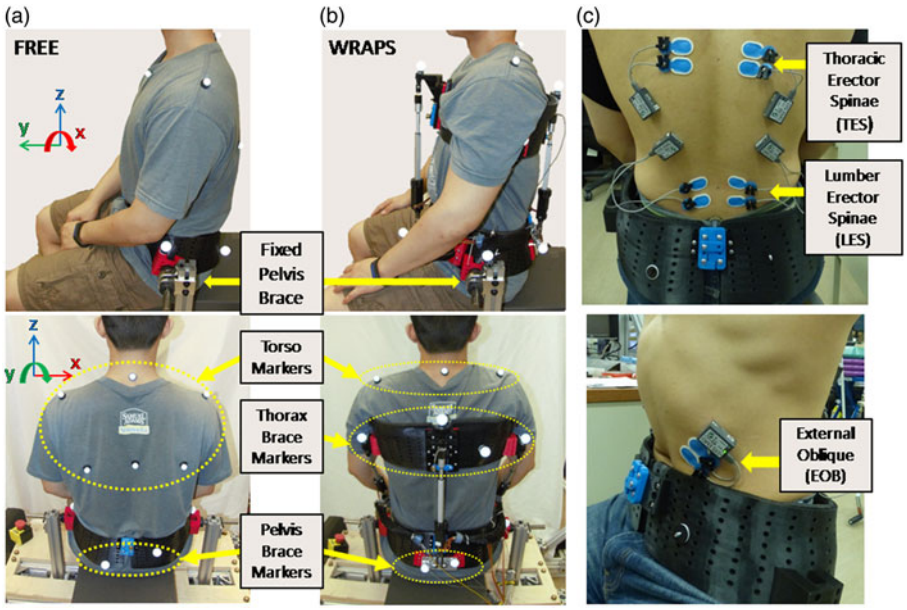


Fig. 5. Experiment setup in (a) "free" session and (b) WRAPS session. (c) Placement of Electromyography (EMG) electrodes on three trunk muscles groups: Thoracic Erector Spinae (TES), Lumbar Erector Spinae (LES), and External Oblique (EOB). The coordinate frames roughly show the pelvis brace orientation in the figures.

Once the "free" session was completed, the subjects wore WRAPS (Fig. 5(b)). The size of the WRAPS brace was adjusted and extra padding with semi-rigid foam was used to ensure the snug fit of the device on each subject. In the WRAPS session, the same three movement directions as in the "free" session were performed: flexion-extension, lateral rotation, and combined motion (using all four DOFs of the device). Each movement was performed once in each of the two modes of the device in sequence as follows:

- Transparent Mode: the subject wore the WRAPS in the zero-force control mode, where the desired wrench $\boldsymbol{W}_{des}$ was set to be the zero vector, resulting in zero desired joint forces along all limbs, and thus the robot performed movements that complied with the forces exerted by the subject on the thorax brace. The initial sitting posture when wearing the WRAPS was determined by the subject using this control mode. Then, the subject was instructed to perform the trunk movements to the maximum range of motion allowed by WRAPS. A metronome was used to pace trunk movements.
- Assistive Mode: the WRAPS was switched to the position control mode and was commanded to follow the tROM trajectories previously recorded during the transparent mode, copying the physiological trunk motion of the subjects in the device. The subjects were verbally instructed to relax their torso muscles and avoid any voluntary trunk movement as the WRAPS followed the recorded trajectory.

Kinematics data were gathered via the control system of WRAPS together with additional measurements:

2.4.1. Motion capture system. A set of eight motion capture system cameras (Vero v2.2, Vicon Motion Capture Systems, Oxford, UK) was used to track the motion of torso and the braces at 100 Hz. Marker placements during the "free" session corresponded to the anatomical landmarks proposed (Ref. [11]) to track the position and the orientation of the trunk: suprasternal notch, xiphoid process, C7 and T8 spinous processes, right–left inferior angles of scapulae, and right–left acromion processes. Furthermore, five markers were also placed on the pelvic ring (Fig. 5(a)). In the WRAPS session (Fig. 5(b)), only four markers were left on the subject's torso (suprasternal notch, C7, and right–left acromion processes) and 11 markers were placed on the pelvis and the thorax rings of the WRAPS.

https://doi.org/10.1017/S0263574719000948 Published online by Cambridge University Press

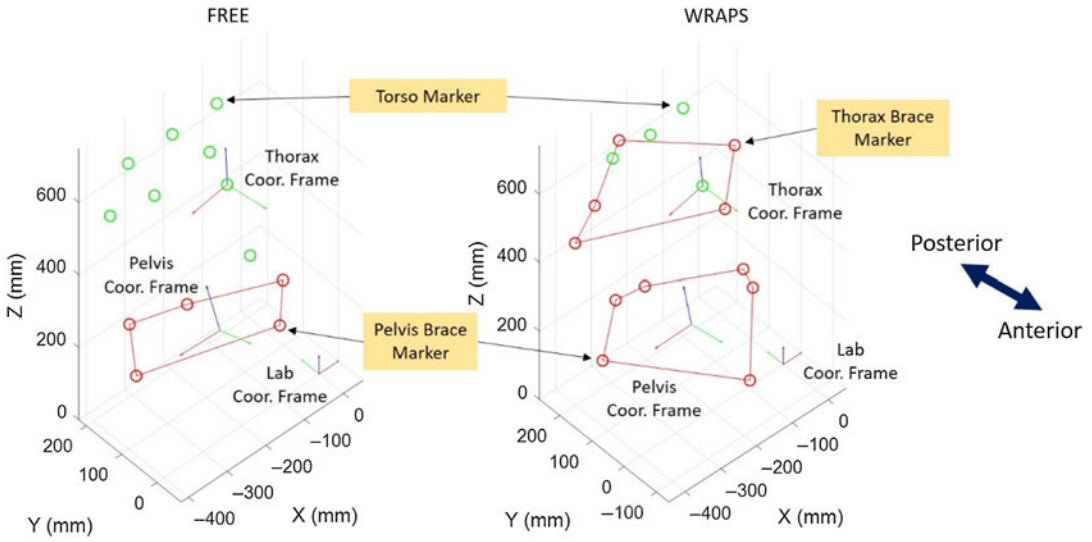


Fig. 6. Vicon marker positions and constructed coordinate frames in a torso neutral configuration.

2.4.2. EMG sensors. The overall muscle activity in the trunk was measured by surface EMG (sEMG). A wireless EMG system (TeleMyo^{TM} Desktop Direct Transmission System (DDTS), Noraxon, AZ, USA) with sampling at 1500 Hz was used along with six electrode channels. The placements of the electrodes for measuring the sEMG of the muscle groups on the trunk were selected as suggested in Refs. [12–14]. The electrodes were placed bilaterally on three muscle groups as shown in Fig. 5(c):

- Thoracic Erector Spinae (TES): 5 cm lateral to the T9 spinous process;
- Lumbar Erector Spinae (LES): 3 cm lateral to the L3 spinous process; and
- External Oblique (EOB): approximately 15 cm lateral to the umbilicus or just below the rib cage, along a line connecting the most inferior costal margin and the contralateral pubic tubercle.

Note that this selection of the positions of the electrodes prevents the electrodes from being compressed by the brace and minimizes artifacts recorded in the EMG signal. Some areas of the skin were shaved as necessary to improve the quality of the interface contact with the electrodes.

In addition, all recorded data from sEMG and the motion capture system were synchronized by using an analog sync box (Lock Lab, Vicon Motion Capture Systems, Oxford, UK). The motion capture software (Nexus 2.5, Vicon Motion Capture Systems, Oxford, UK) commanded the sync box to send a continuous high analog signal to the WRAPS control board and the wireless receiver of the EMG system during the data capture. Only the portion of recorded data with high analog sync signal was used.

2.5. Data analysis

2.5.1. Upper torso kinematics. The torso coordinate system was constructed by using marker positions on the anatomical landmarks, based on a guideline from Ref. [11]. The coordinate frame of the pelvis ring center was determined from marker positions in the 3D assembly model of the brace in a CAD software. A visualization of all coordinate systems in both sessions is presented in Fig. 6. We evaluated the kinematics of the upper torso of the subject by finding the transformation from the pelvic coordinate frame to the thorax coordinate frame. The output translational displacement (x, y, z) is from the pelvis frame origin to the thorax frame origin (the suprasternal notch), and the orientation of the thorax frame is in space-three 1-2-3 set of orientation angles $(\psi_x, \theta_y, \phi_z)$, corresponding to pitch-roll-yaw motion of the upper trunk. Figure 7 shows an example of the processed trunk kinematics data in one movement of a subject for both the "free" and the WRAPS transparent trials. Figure 7(a) shows all six variables over time, and Fig. 7(b) shows the trajectories of the WRAPS in the transparent mode overlaid with the trajectory in the "free" mode.

https://doi.org/10.1017/S0263574719000948 Published online by Cambridge University Press

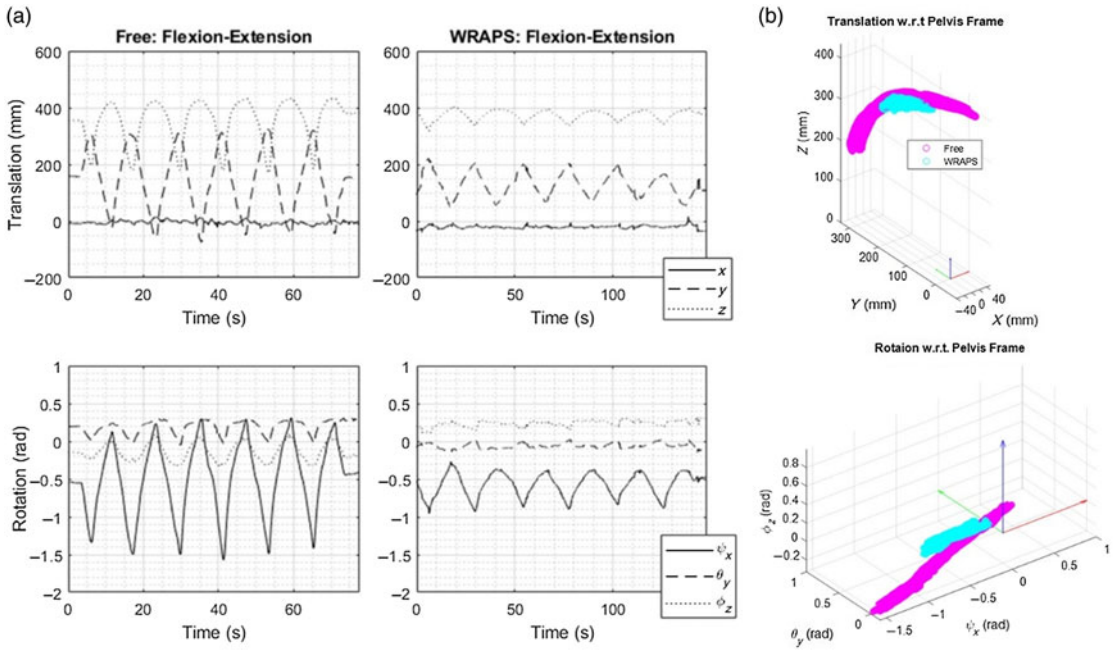


Fig. 7. Kinematics data of the torso flexion-extension movement of one representative subject with respect to the pelvis coordinate frame in both the "free" and the transparent trials in (a) all six DOFs over time and (b) the 3D trajectories of the translation and rotation over the entire movement.

In order to calculate the tROM, we averaged the peaks of its dominant DOFs, namely (y, z, ψ_x) in the flexion-extension, and $(x, -z, \theta_y)$ in the lateral rotation. The peaks were found in both positive and negative directions relative to the starting position in each trial. The tROM in each DOF was calculated as a percentage of the average peak in the WRAPS session compared to the "free" session.

2.5.2. EMG processing. The EMG processing was performed in myoRESEARCH® software (MR3.12, Noraxon, AZ, USA) and MATLAB® (R2018b, MathWorks, Natick, MA, USA) using suggested methods from Refs. [6, 15, 16]. First, the electrocardiography data were removed from the raw measurement, and then the data were detrended to remove the DC-offset of the signal. After this the band-pass filter of 30–500 Hz was applied to the signal, and then the band-stop filter (58–62 Hz) was applied to remove the artifacts from the power line. The signal was then rectified and root-mean-square enveloped over the 500-ms sliding window. The signal magnitudes were normalized based on the maximum value in each channel occurring in the entire experiment.

In Fig. 8, the EMG signal was cut into cycles based on the kinematic data recorded from the WRAPS. Each cycle was specified by the interval from one peak to another in a selected DOF. After this, all cycles were normalized by time. Finally, the summed integrated EMG data over the normalized time from the right and left muscles were averaged over the five cycles, representing the normalized EMG activity of each muscle group corresponding to a trial. Note that the kinematics of the WRAPS in both conditions were slightly different due to the delay from the time constant of the PID controller and different load conditions.

2.6. Statistical analysis

The statistical package SPSS® (version 25, IBM, Armonk, NY, USA) was used for statistical analyses of the normalized EMG data between the transparent and assistive modes of the WRAPS. Data normality was explored with Q-Q plots and Shapiro–Wilk test. The alpha rate was set at 0.05 as significance level. For our single subject test, we used relative change with respect to baseline to describe WRAPS functionality in transparent and assistive modes within the same movement. In our group analysis ($n = 5$), paired sample t-tests were used to examine significant differences. One subject was removed from the EMG analysis due to technical issues, as determined by extreme data outliers (three times greater than the interquartile data range).

https://doi.org/10.1017/S0263574719000948 Published online by Cambridge University Press

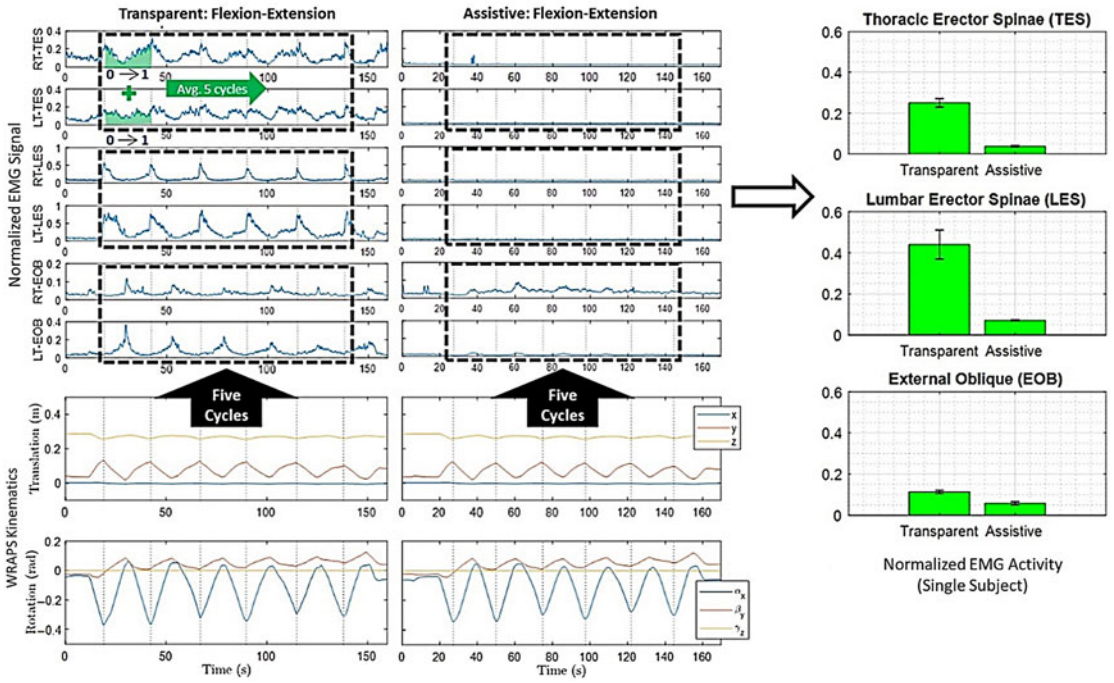


Fig. 8. EMG processing of the flexion-extension movement of a subject wearing the WRAPS in the transparent and the assistive trials. Five cycles were determined by using the minimum peaks of the flexion-extension angles (α_x).

3. Results and Discussions

3.1. tROM: "Free" versus WRAPS sessions

The tROM of the WRAPS in the transparent mode is compared to the tROM in the "free" mode in percentage of the average peak values. The group average %tROM in each DOF was calculated from two subjects with complete motion capture data (Fig. 9). Each DOF has two values of %tROM in positive and negative directions starting from the neutral configuration.

In Fig. 9(a), WRAPS can achieve a higher %tROM in the flexion ($+y$, $-z$, $-\psi_x$) than the extension movement ($-y$, $+z$, $+\psi_x$). The device can achieve relatively high %tROM in the forward translation ($+y$) as well as the flexion angle ($-\psi_x$) at $69.0\% \pm 4.5\%$ and $47.5\% \pm 10.6\%$, respectively. These outcomes indicate that the WRAPS can efficiently support the body and provide an in-device forward reaching distance very close to the user's natural reach. WRAPS was principally designed to expand the subject's functional reach space in the forward direction while proving comfortable and active full body weight support. The vertebral column is highly unstable in the vertical position,[17] and the absent neuromuscular control of paravertebral muscles during extension movements may be the cause of further neural or soft tissue injuries in people which SCI caused by hypertension mechanisms.[18]

In Fig. 9(b), the lateral rotation in the WRAPS achieved uniform %tROM across all major DOFs of the movement. The average %tROM in lateral translation (x) achieved relatively symmetric values ($40.0\% \pm 9.4\%$ and $42.5\% \pm 7.8\%$ in positive and negative directions, respectively). The downward translation ($-z$) also has the average %tROM ($40.0\% \pm 17.1\%$) close to other DOFs. The slightly asymmetric %tROM of lateral bending angles ($45.0\% \pm 13.2\%$ and $28.5\% \pm 9.8\%$ on the right and left side, respectively) may be due to an offset neutral angle around the y axis of the device. Also, the %tROM can significantly vary by different pelvis and thorax ring sizes across the subjects. The subjects with wider ring sizes tend to have less %tROM during the lateral rotation movement since the linear actuators in the UPS chains will have to reach longer lengths for the same angle of torso lateral rotation (θ_y).

https://doi.org/10.1017/S0263574719000948 Published online by Cambridge University Press

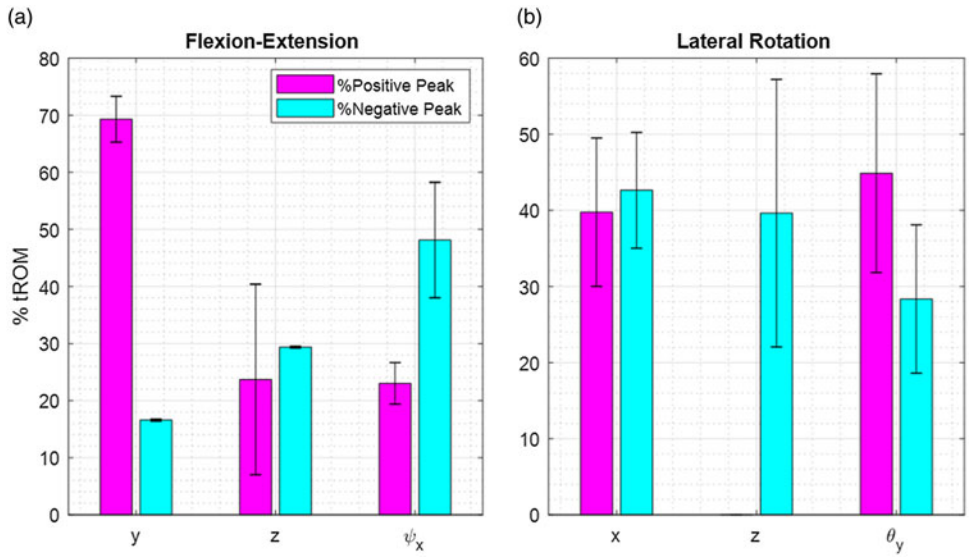


Fig. 9. Average %tROM ($n = 2$) in the WRAPS compared to the "free" conditions in (a) flexion-extension and (b) lateral rotation movements.

3.2. Assistive forces and moment versus muscle activation pattern

During the assistive mode (position controller), the peak forces along the actuators when interacting with the subjects were always below the back drive force (102 N), and thus the robot was able to track the desired trajectories throughout the experiment. The peak forces that occurred throughout the experiment were 87.48 N in compression along the lateral UPS leg, and 90.83 N in tension along the rear RPS leg. The maximum peak forces occurred during the assisted flexion-extension were 80.77 N in compression along the rear RPS leg and at 70.66 N in tension along a lateral UPS leg.

Since the structure of the robot was specifically designed to control and measure forces and moment in the sagittal plane, the recorded force data were exclusively correlated with the assisted flexion-extension movement. The joint forces, end-effector wrench, and kinematics data measured by the WRAPS of a representative subject are shown in Fig. 10(a). Positive and negative joint forces correspond to axial tension and compression forces, respectively. The forces and moment shown are in the direction applied on the end-effector from interaction with the wearer. The time points at which the robot reached its extreme flexion angle are shown by vertical dotted lines. Given that all muscle activities in this healthy subject, shown in Fig. 10(b), have decreased (−28.2% in TES, −37.4% in LES, and −32.3% in EOB), the characterization of the assistance provided by the WRAPS in this case could be related to the patient group with low muscle strength in the torso.

There are distinct trends of the end-effector sagittal forces (F_y, F_z) and the moment (M_x) during this cyclic flexion-extension motion. For easier interpretation of the data, the kinematic and force-moment data of the representative subject in Fig. 10(a) were averaged throughout the five time-normalized cycles and then shown in Fig. 10(c). The unique characteristic of the assistive forces and moment were delineated in four consecutive phases of the movement as follows.

3.2.1. Flexion to neutral phase (0–25% of Cycle). In the third plot from the left in Fig. 10(c), the resultant sagittal force vector $\boldsymbol{F} = [0, F_y, F_z]^T$ on the torso (opposite direction of the forces shown in the plot) started from the forward direction due to the guiding force in the previous cycle that assisted the torso to reach the terminal flexion angle. After that, the force shifted toward the posterior and inferior direction (pulling torso backward and downward) in order to adjust the body back to the neutral configuration. It can be observed that joint force along the rear RPS limb changed from compression at the 0% of the cycle to the tension at the end of this phase. This joint force profile was similar to the main activation pattern of the LES muscle during the same phase of motion in the transparent mode as seen in Fig. 8. The onset of peak activation by the TES and LES muscle was immediately after the extreme flexion motion and remained high shortly afterwards. It could be concluded that the substantial decrease of required muscle activity in the LES was contributed by this assistive joint force. Note that the magnitude of the tension force along the rear RPS limb

https://doi.org/10.1017/S0263574719000948 Published online by Cambridge University Press

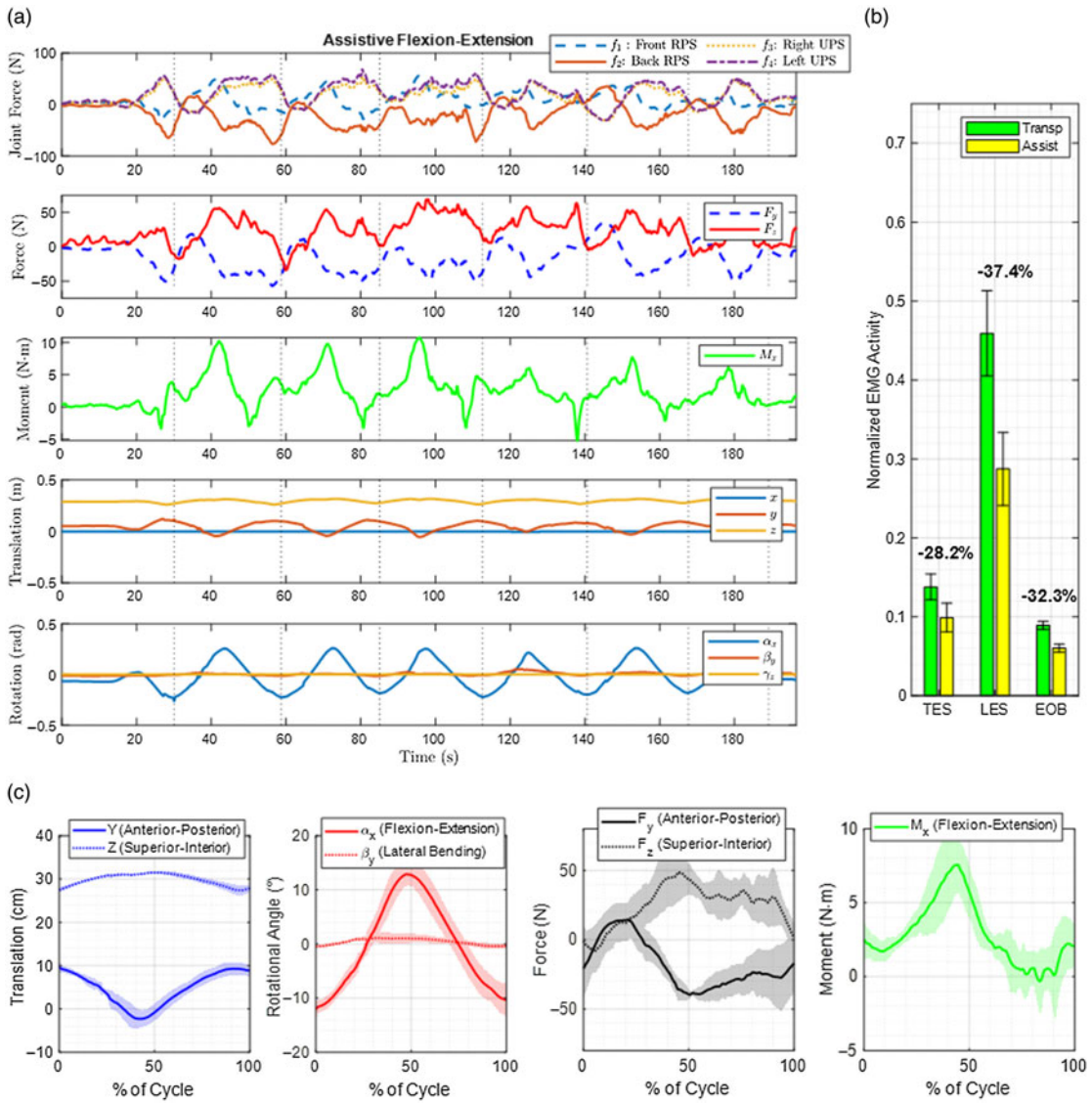


Fig. 10. (a) Joint forces along limbs and sagittal forces and moment at the center of the thorax brace in the assisted flexion-extension session in a representative subject. Dotted lines indicate the time when the WRAPS reached the extreme flexion motion. Positive and negative joint forces correspond to in-line tension and compression forces, respectively. The forces and moment shown are the force applied on the end-effector by the wearer. (b) Normalized EMG activities of three muscle groups during transparent and assistive modes with relative percentage differences based on the transparent mode. (TES: Thoracic Erector Spinae; LES: Lumbar Erector Spinae; EOB: External Oblique). (c) Average kinematics and force-moment data in five cycles of the same subject (one extreme flexion angle to another) with $\pm 1SD$ bands. The WRAPS reached the maximum flexion angle at 0% and 100% of the cycle.

was relatively low, possibly due to the additional compressive force from the torso inertia when it was shifted backward. Interestingly, the moment from the inertia of the torso rotating backward was greater than the gravitational torque from the weight of the torso, resulting in the small positive value of flexion-extension moment reaction on the WRAPS.

3.2.2. Neutral to extension phase (25%–50% of Cycle). The direction of the F_y and F_z rapidly diverged from each other at the beginning of the cycle. The F_y returned to the negative direction again, meaning that after the sagittal angle (α_x) of the thorax ring had shifted to the positive direction (extension), the subject's torso weight immediately shifted backward until the F_y reached its peak at around -40 N at the extreme extension angle. Meanwhile, the increase in the positive vertical

https://doi.org/10.1017/S0263574719000948 Published online by Cambridge University Press

reaction force F_z on the end-effector was mainly due to the extension of the spinal column, which overcame the downward gravitational force of the torso. In contrast, the sagittal moment reached its peak at the end of this phase, reflecting the gravitational moment from the fully extended torso. During extension movements, it can be concluded that the subject's torso weight was shifted backwards, and the WRAPS had a major role in supporting the upper body in the vertical position. This biomechanical effect was observed during low, or almost inexistent, EMG activity abdominal muscles (EOB) that were used to stabilize the reclining motion during the transparent mode. This is an important finding in WRAPS since people with total low-cervical or high-thoracic SCI do not have muscle stabilization of the torso and passive orthosis could not offer this active regulation of compression forces in vertical or during active extension movements. Furthermore, it was reasonable to observe that the front RPS and the lateral UPS limbs that have the configurations similar to the abdominal muscles, like the Rectus Abdominis and the EOB, respectively, are dominantly under the tension at the terminal extension angle. This pattern is supported by the representative data in Fig. 8, which shows that both left and right EOBs reached their peak activity when the torso is fully extended in the WRAPS.

3.2.3. Extension to neutral phase (50%–75% of Cycle). The magnitude of the sagittal force vector slightly decreased while the torso was moving back to the neutral configuration (more neutral spinal column). At the same time, the gravitational moment M_x on the end-effector rapidly decreased during this phase to nearly zero. This outcome is well related with the noticeable reduction of the tension force along the front RPS leg when the gravitational moment was disengaged (Fig. 10(a)), while the lateral UPS legs were still maintaining more tension throughout this phase since their diagonal vectors were more aligned with the partially extended upper spinal column and also mainly contributed to the end-effector anterior force that push the body forward to the neutral position.

3.2.4. Neutral to flexion phase (75%–100% of Cycle). The main reaction force was still in the backward direction since the WRAPS was pushing the torso forward to the flexion posture; meanwhile, the gravitational moment M_x from the torso shifted more into the negative direction. Interestingly, the resultant moment magnitude in the negative direction was still relatively low since the positive reaction moment from the effort by the robot trying to bend the body forward significantly compensated the gravitational moment from the torso.

In summary, during the represented subject's assisted flexion-extension motion in the WRAPS, we can conclude that during the first phase (0%–25%), the rear RPS limb can serve to supply the absent activity of the erector spinae muscle group in people with SCI to extend the torso back to the neutral configuration. In the second phase (25%–50%), the front RPS limb and the lateral UPS limbs acted like the abdominal muscle groups which stabilized the torso when reaching the fully extended position. In the last two phases (50%–100%), the front RPS limb exclusively controlled the flexion-extension moment on the torso, while the steady vertical and horizontal force components that mobilized the torso forward were specifically controlled by the tensions along the lateral UPS limbs, favored by their symmetrical and diagonal configuration in the sagittal plane. In Fig. 10(a), the joint forces along the lateral UPS limbs (f_3, f_4) are nearly the same in both directions and magnitudes throughout the entire movement. This means that if the recorded movement during the transparent mode is symmetrical around the sagittal plane, the design of the WRAPS will maintain equally distributed forces among the actuators around the sagittal plane when displacing the torso through the copied trunk movement. This design merit may provide additional vertebral stability of the WRAPS user.

These observed patterns may slightly vary with differences in anthropometric measurements as well as the movement speeds. It is also important to note that the representative subject had the same range of flexion and extension angles in the device. This tROM was based on the self-selected neutral configuration of the subject. In addition, the cyclic movements in this experiment were continuous, which might be different from normal seated tasks that involve prolonged static postures, such as reaching something on a shelf. Nevertheless, the synergies between the actuations and the kinematics of the trunk found in this experiment could be potentially generalized to a template for patients with similar anthropometry.

https://doi.org/10.1017/S0263574719000948 Published online by Cambridge University Press

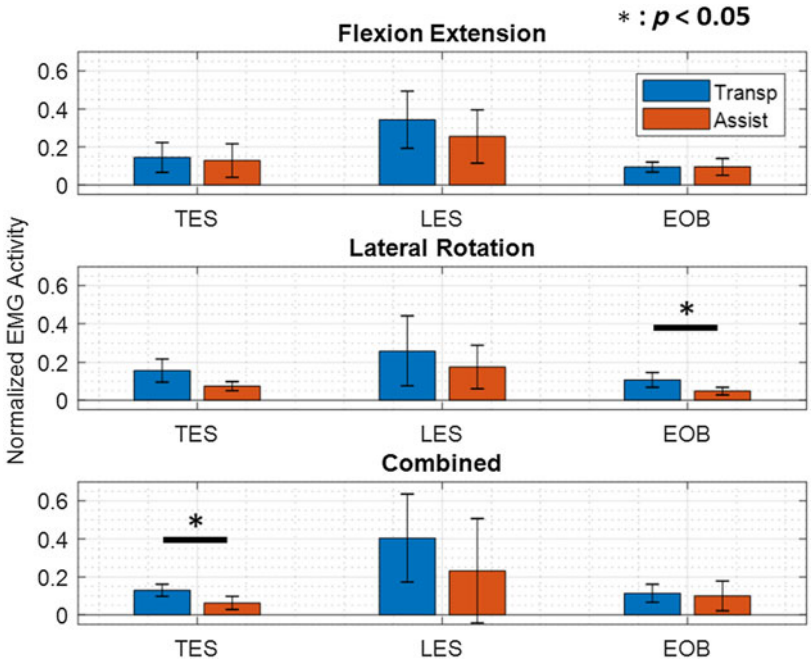


Fig. 11. Subject group average ($n = 4$) of the normalized EMG activity on each muscle group during three movements.

3.3. Group comparison of sEMG between transparent versus assistive modes

The average normalized sEMG activity for each muscle group across cycles in the three different movements was analyzed (Fig. 11). The EMG data show a general trend of reduced muscle activity during the assistive mode. Furthermore, statistical significance was found between the two WRAPS modes of control for specific muscle groups. The normalized EMG activity of TES was significantly reduced during the combined movements in the assistive mode (M = 0.062, SD = 0.034) compared to the transparent mode (M = 0.129, SD = 0.031); $t = 3.25$ (3), $p = 0.048$. Similarly, in the assistive mode, there was a significant decrease of the normalized EMG activity in the EOB muscle group during lateral rotation movements (M = 0.048, SD = 0.020) that was not found with the transparent mode (M = 0.106, SD = 0.038); $t = 3.66$ (3), $p = 0.035$.

The reason we do not see statistically significant reduction of the average EMG activity throughout all muscle groups may be due to different strategies that healthy subjects used to move the brace in the transparent mode. Some subject might already have minimized their muscle activation because of high sensitivity of the zero-force controller. The speed of the metronome of some subjects was adjusted to be slightly slower to ensure that the subjects could reach their extreme positions in the brace while keeping up with a tempo, which might be a reason why these subjects produced only marginally higher EMG activity in the transparent mode respective to the assistive mode. Furthermore, the subject-based normalization technique that was used may provide inconsistency in the ranges of calculated normalized muscle activity. Tuning controller gains based on perception and strategy of each subject may also lead to different EMG activity levels. It is also interesting to investigate the EMG activity during the "free" movement in comparison with the WRAPS conditions; the speed of the movement and the tROM have to be similar in order to the make the EMG activity comparable across these two conditions.

4. Conclusions

We examined in seated healthy subjects the trunk range of motion in the sagittal and frontal planes with WRAPS in two modes: transparent (i.e., zero force control mode) and assistive mode (position control). The data from these two modes were compared with the condition without WRAPS ("free" condition). In summary, WRAPS was able to safely and comfortably sustain and stabilize the

https://doi.org/10.1017/S0263574719000948 Published online by Cambridge University Press

concomitant active forces resulting from the torso of healthy young adults (mean = 71.55 kg) during assisted trunk motion. No major complaints (i.e., pain or excessive paravertebral muscle fatigue) were reported by the subjects. Our outcomes show that WRAPS can accommodate trunk trajectories that are close to physiological trunk ROM in sitting position along the sagittal and frontal planes, considering the hardware limitations. Furthermore, the position control mode can be efficiently applied to guide the torso throughout the planar trajectories that copy torso movements registered during the transparent mode. Importantly, our sEMG data demonstrate that WRAPS can reproduce such trunk trajectories with a significant reduction in EMG activity of primary torso muscles, which is a condition expected in people with SCI. Moreover, the WRAPS actuation pattern is mechanically closely related to the spatiotemporal activation of abdominal and erector spinae muscle groups, and thus, it may be used to replace such muscle function in people with SCI without trunk muscle control. Altogether, these preliminary observations open new frontiers in the future safe and efficient application of WRAPS in patients with neuromotor disorders and profound trunk control deficits like SCI at cervical or high-thoracic levels, spina bifida, cerebral palsy with severe axial hypotonia, and neuromuscular conditions.

As a limitation, only male subjects participated in the present study. Therefore, future work will aim at the improvement in the adjustability and the ergonomics of the WRAPS to fit both genders and a wider range of torso dimensions. An admittance-based controller can be implemented in future as an alternative to the direct PID force controller to improve the stability and robustness when the system is interacting with healthy subjects, while the impedance-based controller can be used during the assistive mode to improve the interaction forces with the wearer. As a statistical note, we think that the lack of power due to low sample size could be masking the presence of further significant EMG activity reductions during the assistive mode.

Furthermore, the user intention via an external manipulandum, like a joystick, will be incorporated into the control of the robot to offer independence and greater level of motor flexibility to users with absent trunk control. An upper-body motion mode recognition from inertia measurement units with machine learning algorithms (Ref. [19]) can potentially be combined with an assist-as-needed controller to encourage functional activities performed by population with partial trunk motor impairment like cerebral palsy patients to encourage healthy postures and delay the muscle atrophy.

It is also interesting to investigate the change in the pressure distribution in the gluteal region when the WRAPS is guiding the torso in different movements. Velocities and acceleration profiles of the devices with the trunk movements also remain to be explored in the future.

Acknowledgments

This work was supported by National Science Foundation (Grant No. IIS-1527087). Additional funding was provided by Beijing Goodoing Speed Smart, Co. The authors would also like to thank Joon-Hyuk Park, Ph.D., for his initial design of the torso braces.

References

1. "Spinal Cord Injury Facts and Figures at a Glance 2018," National SCI Statistical Center, Birmingham, AL (2018).
2. E. B. Forslund, K. S. Roaldsen, C. Hultling, K. Wahman and E. Franzén, "Concerns about falling in wheelchair users with spinal cord injury-validation of the swedish version of the spinal cord injury falls concern scale," *Spinal Cord* **54**(2), 115–119 (2016).
3. E. B. Forslund, V. Jørgensen, E. Franzén, A. Opheim, Å. Seiger, A. Ståhle, C. Hultling, J. K. Stanghelle, K. S. Roaldsen and K. Wahman, "High incidence of falls and fall-related injuries in wheelchair users with spinal cord injury: A prospective study of risk indicators," *J. Rehabil. Med.* **49**(2), 144–151 (2017).
4. N. Sezer, S. Akkuş and F. G. Uğurlu, "Chronic complications of spinal cord injury," *World J. Orthop.* **6**(1), 24 (2015).
5. T. Ogura, T. Itami, K. Yano, I. Mori and K. Kameda, "An Assistance Device to Help People with Trunk Impairment Maintain Posture," **In**: *Proceedings of the IEEE International Conference on Rehabilitation Robotics*, London, UK (2017) pp. 358–363.
6. M. N. Mahmood, L. H. C. Peeters, M. Paalman, G. J. Verkerke, I. Kingma and J. H. van Dieën, "development and evaluation of a passive trunk support system for duchenne muscular dystrophy patients," *J. Neuroeng. Rehabil.* **15**, 22 (2018).
7. R. C. Murray, C. Ophaswongse and S. K. Agrawal, "Design of a Wheelchair Robot for Active Postural Support," **In**: *Proceedings of the ASME International Design Engineering Technical Conferences and Computers and Information in Engineering Conference*, Anaheim, CA (2018) pp. V05AT07A059.

https://doi.org/10.1017/S0263574719000948 Published online by Cambridge University Press

8. C. C. Nguyen, S. C. Antrazi, Z. L. Zhou and C. E. Campbell, "Analysis and implementation of a 6 DOF stewart platform-based robotic wrist," *Comput. Electr. Eng.* **17**(3), 191–203 (1991).
9. L. W. Tsai, *Robot Analysis: The Mechanics of Serial and Parallel Manipulators* (John Wiley & Sons, Inc., New York, NY, 1999).
10. D. Gan, J. S. Dai, J. Dias, R. Umer and L. Seneviratne, "Singularity-free workspace aimed optimal design of a 2T2R parallel mechanism for automated fiber placement," *J. Mech. Robot.* **7**(4), 41022–41029 (2015).
11. G. Wu, F. C. Van der Helm, H. D. Veeger, M. Makhsous, P. Van Roy, C. Anglin, J. Nagels, A. R. Karduna, K. McQuade, X. Wang and F. W. Werner, "ISB recommendation on definitions of joint coordinate systems of various joints for the reporting of human joint motion–Part II: shoulder, elbow, wrist and hand," *J. Biomech.* **38**(5), 981–992 (2005).
12. M. S. McGill, "Electromyographic activity of the abdominal and low back musculature during the generation of isometric and dynamic axial trunk torque: implications for lumbar mechanics," *J. Orthop. Res.* **9**(1), 91–103 (2005).
13. L. Danneels, P. Coorevits, A. Cools, G. Vanderstraeten, D. Cambier, E. Witvrouw and H. De Cuyper, "Differences in electromyographic activity in the multifidus muscle and the iliocostalis lumborum between healthy subjects and patients with sub-acute and chronic low back pain," *Eur. Spine J.* **11**(1), 13–19, (2002).
14. K. O'Sullivan, R. McCarthy, A. White, L. O'Sullivan and W. Dankaerts, "Lumbar posture and trunk muscle activation during a typing task when sitting on a novel dynamic ergonomic chair," *Ergonomics* **55**(120), 1586–1595 (2012).
15. M. S. Redfern, R. E. Hughes and D. B. Chaffin, "High-pass filtering to remove electrocardiographic Interference from torso EMG recordings," *Clin. Biomech.* **8**(1), 44–48 (1993).
16. P. Konrad, *The ABC of EMG: A Practical Introduction to Kinesiological Electromyography ver 1.4*, (Noraxon U.S.A. Inc., 2006) pp. 1–61.
17. M. Panjabi, K. Abumi, J. Duranceau and T. Oxland, "Spinal stability and intersegmental muscle forces. A Biomechanical model," *Spine (Phila Pa 1976)* **14**(2), 194–200 (1989).
18. H. Kinoshita, "Pathology of hyperextension injuries of the cervical spine," *Spinal Cord* **32**(6), 367 (1994).
19. P. S. Sun, J. Mai, Z. Zhou, S. K. Agrawal and Q. Wang, "Upper-Body Motion Mode Recognition Based on IMUs for a Dynamic Spine Brace," **In**: *Proceedings of the IEEE International Conference on Cyborg and Bionic Systems*, Shenzhen, China (2018) pp. 167–170.

https://doi.org/10.1017/S0263574719000948 Published online by Cambridge University Press